NASA TECHNICAL NOTE

NASA TN D-3827

NASA TN D-3827

AERODYNAMIC CHARACTERISTICS AT MACH 2.03 OF A SERIES OF CURVED-LEADING-EDGE WINGS EMPLOYING VARIOUS DEGREES OF TWIST AND CAMBER

by Barrett L. Shrout

Langley Research Center
Langley Station, Hampton, Va.

NATIONAL AERONAUTICS AND SPACE ADMINISTRATION • WASHINGTON, D. C. • FEBRUARY 1967

NASA TN D-3827

AERODYNAMIC CHARACTERISTICS AT MACH 2.03 OF A SERIES OF CURVED-LEADING-EDGE WINGS EMPLOYING VARIOUS DEGREES OF TWIST AND CAMBER

By Barrett L. Shrout

Langley Research Center
Langley Station, Hampton, Va.

NATIONAL AERONAUTICS AND SPACE ADMINISTRATION

For sale by the Clearinghouse for Federal Scientific and Technical Information
Springfield, Virginia 22151 – Price $1.00

AERODYNAMIC CHARACTERISTICS AT MACH 2.03 OF A SERIES OF CURVED-LEADING-EDGE WINGS EMPLOYING VARIOUS DEGREES OF TWIST AND CAMBER

By Barrett L. Shrout
Langley Research Center

SUMMARY

A series of curved-leading-edge wings employing various degrees of twist and camber was tested in the Langley 4- by 4-foot supersonic pressure tunnel at a Mach number of 2.03 and a Reynolds number, based on the mean geometric chord, of 4.4×10^6. The results are compared with theoretical predictions. Maximum lift-drag ratios predicted by theory were not attained experimentally although the wings twisted and cambered for an intermediate design lift coefficient yielded higher experimental values of maximum lift-drag ratio than did the corresponding flat wings.

Comparison of the variation of some of the aerodynamic parameters with planform exponent K, which indicates the amount of curvature in the leading edge, showed an increase in lift-curve slope and a slight increase in stability with increasing K. In addition, there is a slight decrease in zero-lift pitching moment with increasing K for the twisted and cambered wings.

INTRODUCTION

The use of twist and camber to improve the design point performance of wings at supersonic speeds has been shown to be effective when used in conjunction with highly swept arrow wing planforms (ref. 1). The design of the camber surface required to support a combination of loadings yielding a minimum drag at a given lift coefficient may be accomplished by a machine computing program based on a numerical application of linearized theory. (See ref. 2.) The camber surfaces so designed for arrow wings are characterized by the steep slopes of the camber surface in the root-chord region behind the planform-apex discontinuity. Such steep slopes are likewise characteristic of the camber surface designed for any wing having a discontinuity in the wing leading edge.

Experimental results for twisted and cambered arrow wings have shown a substantial drag reduction at lift over that obtained for flat wings of the same planform. However, these wings have failed to achieve, by a good margin, the full theoretical potential of the

design. This failure is believed to be due in part to the increasing inapplicability of the linearized theory as surface slopes become larger, as in the vicinity of the root chord.

An obvious method for alleviating the severity of the camber-surface slopes in the root-chord region would be to eliminate or, at least, reduce the discontinuity at the leading edge of the root chord. This observation led to the design of a series of wing planforms having convex parabolic leading edges.

The curved-leading-edge planforms do not offer as much theoretical potential for drag reduction at lift, due to twist and camber, as arrow-wing planforms do; however, in practice, a large portion of that potential might be attained since no steep slopes are required. Consideration of the theoretical drag characteristics of the various wings led to the selection of two of the planforms for model construction and wind-tunnel testing. Three wings of each series were constructed with twist and camber corresponding to design lift coefficients of 0, 0.08, and 0.16. (A design lift coefficient of 0 corresponds to a flat wing.) The wings were tested in the Langley 4- by 4-foot supersonic pressure tunnel at a Mach number of 2.03 and a Reynolds number, based on mean geometric chord, of 4.4×10^6.

SYMBOLS

b	wing span
c	chord length
c_r	root chord length
$\bar{c}$	wing mean geometric chord
C_D	drag coefficient, Drag/qS
C_L	lift coefficient, Lift/qS
$C_{L,design}$	lift coefficient for which the wing camber surface is designed to produce a minimum drag in comparison with other wings of the family
C_{L_α}	lift-curve slope per degree, $\Delta C_L/\Delta\alpha$
C_m	pitching-moment coefficient about $\bar{c}/4$, Pitching moment/qS$\bar{c}$
L/D	lift-drag ratio, C_L/C_D

K	planform exponent
m	planform coefficient
M	Mach number
q	dynamic pressure
R	Reynolds number
S	wing area
x,y	Cartesian coordinate system with origin at wing apex, X-axis streamwise
x'	distance rearward from leading edge
z_c	camber surface ordinate, positive up (measured from reference plane)
α	angle of attack, degree

Subscripts:

exp	experimental
max	maximum
o	zero lift

DESIGN CONSIDERATIONS

The desirability of having the wing leading edge swept well behind the Mach line originating at the wing apex in order to avoid transonic flow phenomena and thus to preserve the load distribution for which the camber surface was designed has been discussed in reference 1. The wing models reported in that reference were two families of wings with straight leading edges, one swept back 70° and the other swept back 75°, and with camber surfaces designed for various design lift coefficients from 0 to 0.16. The swept-back straight-leading-edge wings are characterized by a sharp discontinuity at the wing apex; the camber surfaces for design lift coefficients greater than 0, consequently, have steep surface slopes in the vicinity of the root chord. Although the wing with a camber

surface designed for the intermediate design lift coefficient (0.08) showed a considerable improvement over the flat wing of the same planform, the full potential of the wing, predicted by the theory, was not realized. The wing with a camber surface designed for a lift coefficient of 0.16 produced experimental performance only slightly better than the corresponding flat wing. It was believed that the failure of the wings to achieve their full theoretical potential was due in large part to increasing inapplicability of linearized theory to the steep surface slopes in the vicinity of the root chord. Reduction of the apex discontinuity while maintaining high leading-edge sweep angles over most of the wing may be achieved by using a curved-leading-edge planform with low sweep angles at the apex and higher values near the wing tip. For this type of planform, the camber surface in the vicinity of the root chord has less steep slopes and the high sweep angles over the outboard part of the wing help to eliminate transonic flow phenomena.

The use of numerical techniques incorporated in a high-speed digital computer program for design and analysis of camber-surface shapes (ref. 2) makes possible the rapid evaluation of the theoretical potential of arbitrary wing planforms. A series of curved-leading-edge wing planforms satisfying the leading-edge equation $x = my^K$ where K varied from 1.0, for a straight leading edge, to 2.0, for the classic parabola, was thus evaluated. The two planforms selected ($K = 1.375$ and $K = 1.750$) represent a compromise between the theoretical drag-due-to-lift factor $\Delta C_D/\Delta C_L{}^2$, which increased with increasing K, and the steepness of the camber-surface slopes, caused by the severity of the discontinuity at the apex which decreased with increasing K. The wing span and the chord distribution, as well as the airfoil section, were the same as those for the 70° leading-edge-sweep arrow-wing family reported in reference 1.

TESTS AND ACCURACY

The tests were conducted in the Langley 4- by 4-foot supersonic pressure tunnel at a free-stream Mach number of 2.03 and a Reynolds number, based on $\bar{c}$, of 4.4×10^6. Transition strips of No. 60 carborundum grit were applied in bands 0.125 inch (0.317 cm) wide located 0.4 inch (1.01 cm) streamwise back from the leading edge of the wings. After the force tests on each of the wings, drag data were taken at zero lift while systematically reducing Reynolds number to insure that the test Reynolds number was well above the Reynolds number range for transition to fully turbulent flow.

Angle of attack was measured optically through the use of prisms recessed in the wing surfaces.

The Mach number and aerodynamic coefficients are estimated to be accurate within the following limits:

M	±0.02
C_D	±0.0003
C_L	±0.0030
C_m	±0.0010

Although some grit drag is probably present in all the data, the amount of such drag is believed to be within the quoted accuracy of the data; therefore, the experimental data have not been corrected for grit drag.

MODELS AND INSTRUMENTATION

Drawings of the planforms of the two curved-leading-edge wing series are shown in figure 1. Both planforms have an aspect ratio of 2.24 and an area for the full-span wing of 212.94 square inches (1373.8 sq cm). The semispan wings were made of stainless steel and had 3-percent-thick streamwise circular-arc sections wrapped symmetrically about the camber surface. Nondimensional camber-surface ordinates for the two wing series are given in table I.

Each wing planform series consisted of three wings. The camber surface of each wing of a particular planform series was designed to produce a minimum value of drag (in comparison with that produced for other wings in the series) at a certain lift coefficient. These design lift coefficients are 0, 0.08, and 0.16 for the wings of each series.

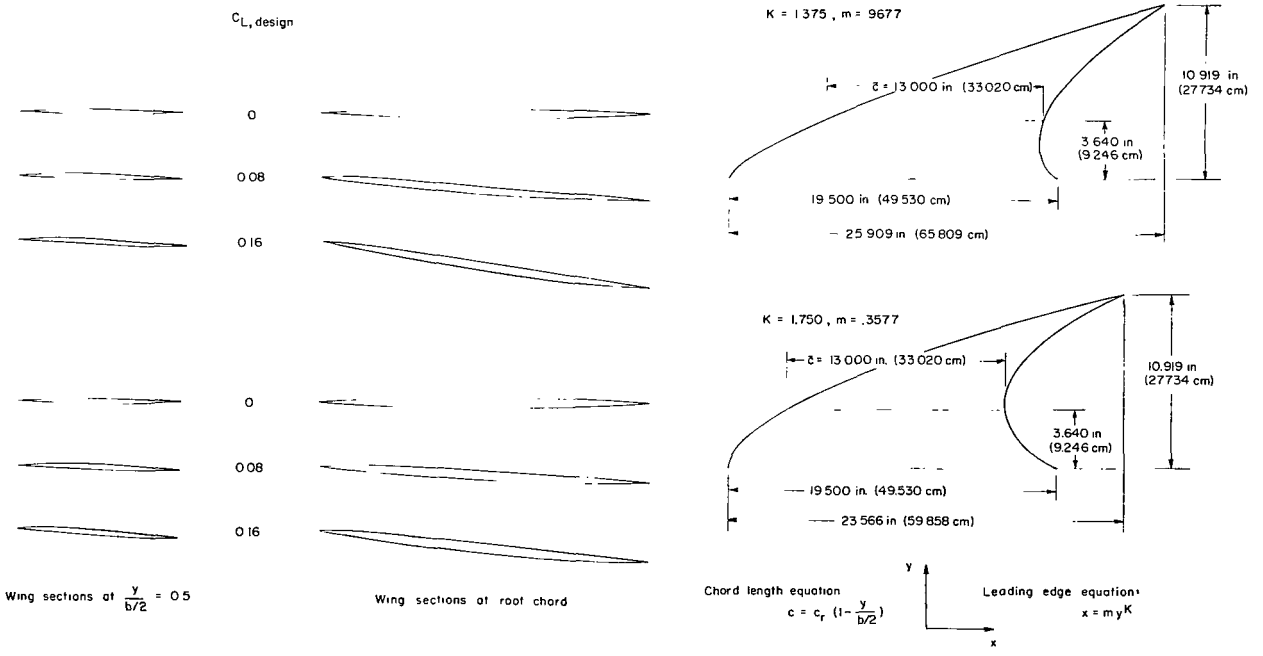

Figure 1.- Typical wing sections and semispan planforms for the two wing series.

TABLE I.- NONDIMENSIONAL CAMBER-SURFACE ORDINATES

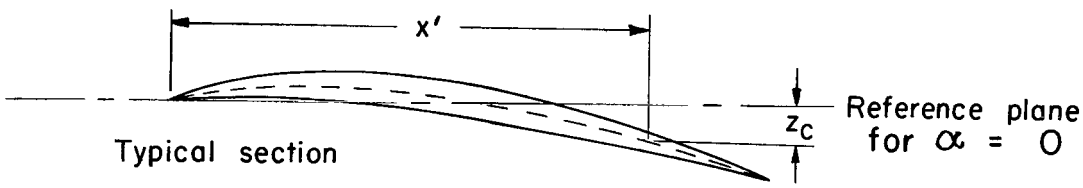

$\frac{x'}{c}$	$\frac{z_c}{c_r C_{L,design}}$ for $\frac{y}{b/2}$ of −													
	0	0.04	0.08	0.12	0.16	0.20	0.30	0.40	0.50	0.60	0.70	0.80	0.90	1.00
K = 1.375														
0	0	0	0	0	0	0	0	0	0	0	0	0	0	0
2.5	-.0164	-.0135	-.0108	-.0087	-.0066	-.0044	.0005	.0039	.0054	.0054	.0049	.0039	.0026	0
5.0	-.0363	-.0271	-.0211	-.0165	-.0124	-.0088	-.0011	.0063	.0100	.0105	.0099	.0079	.0051	0
10.0	-.0829	-.0593	-.0460	-.0369	-.0296	-.0219	-.0068	.0070	.0154	.0171	.0170	.0155	.0100	0
20.0	-.1853	-.1333	-.1056	-.0885	-.0714	-.0568	-.0289	-.0031	.0135	.0218	.0265	.0284	.0191	0
30.0	-.2918	-.2129	-.1714	-.1445	-.1195	-.0981	-.0565	-.0198	.0056	.0205	.0313	.0349	.0271	0
40.0	-.3975	-.2943	-.2399	-.2038	-.1711	-.1433	-.0883	-.0409	-.0064	.0160	.0318	.0394	.0339	0
50.0	-.4998	-.3744	-.3088	-.2640	-.2243	-.1904	-.1224	-.0646	-.0213	.0086	.0308	.0428	.0391	0
60.0	-.5963	-.4525	-.3760	-.3239	-.2776	-.2381	-.1584	-.0905	-.0384	-.0007	.0275	.0440	.0424	0
70.0	-.6855	-.5263	-.4410	-.3823	-.3304	-.2859	-.1951	-.1179	-.0570	-.0119	.0230	.0448	.0448	0
80.0	-.7665	-.5948	-.5024	-.4384	-.3816	-.3328	-.2323	-.1461	-.0771	-.0245	.0173	.0443	.0479	0
90.0	-.8383	-.6575	-.5595	-.4913	-.4306	-.3783	-.2691	-.1750	-.0983	-.0381	.0103	.0430	.0508	0
100.0	-.8996	-.7131	-.6116	-.5403	-.4769	-.4216	-.3055	-.2041	-.1200	-.0528	.0026	.0411	.0523	0
K = 1.750														
0	0	0	0	0	0	0	0	0	0	0	0	0	0	0
2.5	-.0148	-.0144	-.0138	-.0133	-.0124	-.0114	-.0085	-.0047	-.0011	.0021	.0036	.0042	.0028	0
5.0	-.0302	-.0298	-.0273	-.0255	-.0234	-.0209	-.0135	-.0062	.0010	.0054	.0077	.0084	.0063	0
10.0	-.0630	-.0597	-.0550	-.0511	-.0463	-.0407	-.0272	-.0129	.0016	.0117	.0159	.0165	.0095	0
20.0	-.1317	-.1237	-.1132	-.1043	-.0946	-.0837	-.0584	-.0323	-.0081	.0113	.0234	.0299	.0177	0
30.0	-.2015	-.1891	-.1732	-.1593	-.1450	-.1295	-.0931	-.0566	-.0218	.0060	.0264	.0364	.0261	0
40.0	-.2704	-.2539	-.2332	-.2149	-.1962	-.1765	-.1297	-.0330	-.0389	-.0024	.0249	.0404	.0346	0
50.0	-.3371	-.3172	-.2920	-.2699	-.2471	-.2236	-.1673	-.1113	-.0581	-.0130	.0220	.0436	.0403	0
60.0	-.4004	-.3776	-.3490	-.3233	-.2973	-.2701	-.2054	-.1408	-.0789	-.0255	.0170	.0442	.0441	0
70.0	-.4598	-.4346	-.4030	-.3744	-.3456	-.3157	-.2435	-.1709	-.1009	-.0395	.0106	.0443	.0471	0
80.0	-.5141	-.4874	-.4535	-.4229	-.3919	-.3596	-.2808	-.2014	-.1238	-.0547	.0031	.0434	.0501	0
90.0	-.5628	-.5354	-.5003	-.4682	-.4355	-.4013	-.3176	-.2319	-.1473	-.0707	-.0055	.0412	.0532	0
100.0	-.6055	-.5781	-.5422	-.5097	-.4763	-.4406	-.3531	-.2621	-.1713	-.0876	-.0150	.0387	.0553	0

The wings were attached to a four-component strain-gage balance housed within the splitter plate as shown in figure 2. The plate was supported in a horizontal position by the permanent sting mounting system of the Langley 4- by 4-foot supersonic pressure tunnel. Changes in angle of attack were made by moving the plate and wing as a single unit. A clearance of 0.010 to 0.020 inch (0.0254 to 0.0508 cm) was provided between the wing and plate except where the wing attached to the balance.

RESULTS AND DISCUSSION

In order to demonstrate that turbulent boundary-layer-flow conditions prevailed for the tests, the data in figure 3 are presented to show the variation of $C_{D,o}$ with Reynolds

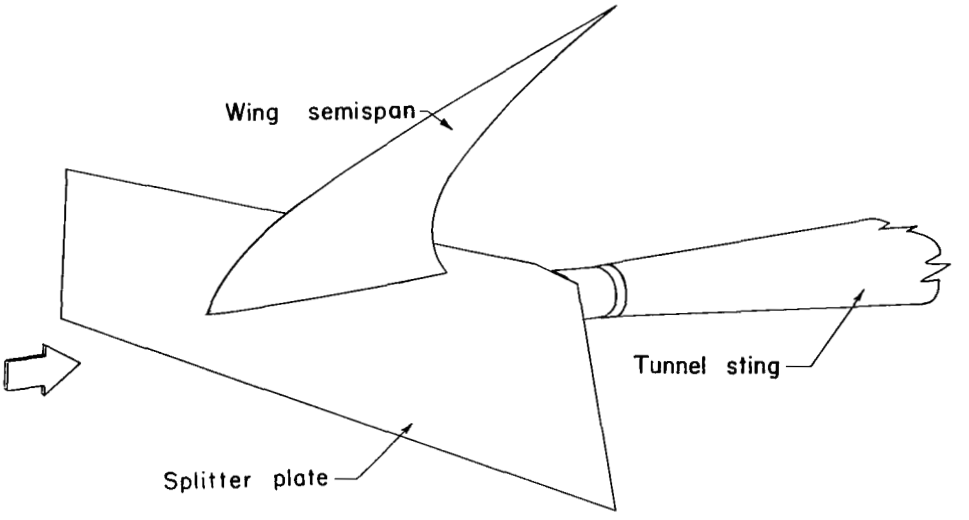

(a) Test rig in tunnel. Upper surface of splitter plate is parallel to tunnel flow.

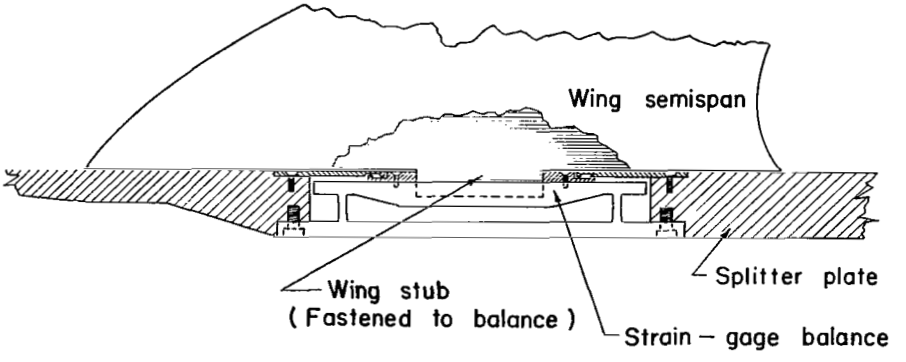

(b) Plate-balance-model details.

Figure 2.- Sketch of test setup.

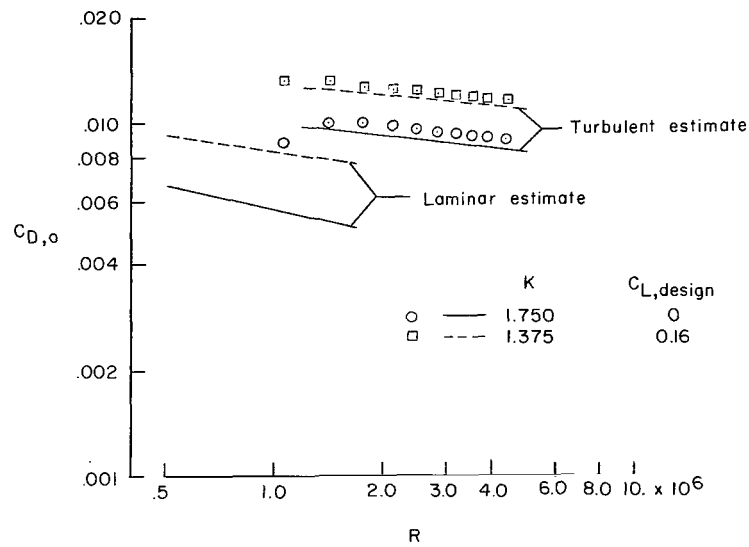

Figure 3.- Variation of $C_{D,o}$ with Reynolds number.

number for two representative wings of the test series. Also shown are estimated values of $C_{D,o}$ for both fully laminar and fully turbulent flow over the wings. Although the drag levels are underestimated in each case, the fact that the data tend to follow the slopes for a fully turbulent boundary layer indicates that transition was fixed and that the flow over the model at the test Reynolds number, based on $\bar{c}$, of 4.4×10^6 was essentially fully turbulent.

The basic longitudinal data for the $K = 1.375$ wings are shown in figure 4. The variations of pitching-moment coefficient and angle of attack with lift coefficient are essentially linear over the lift-coefficient range of this investigation (fig. 4(a)). Significant amounts of positive pitching moment at zero lift for the cambered and twisted wings can be noted. The wing designed for a lift coefficient of 0.08 produced a higher value of $(L/D)_{max}$ than that for the flat wing (fig. 4(b)), but the wing designed for a lift coefficient of 0.16 produced essentially the same value of $(L/D)_{max}$ as the flat wing, although at a somewhat higher lift coefficient.

Basic longitudinal data for the $K = 1.750$ wings are shown in figure 5. Again, for these wings, the variations of pitching-moment coefficient and angle of attack with lift coefficient are essentially linear (fig. 5(a)). Maximum lift-drag ratio for the wing designed for a lift coefficient of 0.08 again is higher than that for the flat wing (fig. 5(b)). For the wing designed for a lift coefficient of 0.16, the maximum lift-drag ratio is slightly less than that for the flat wing.

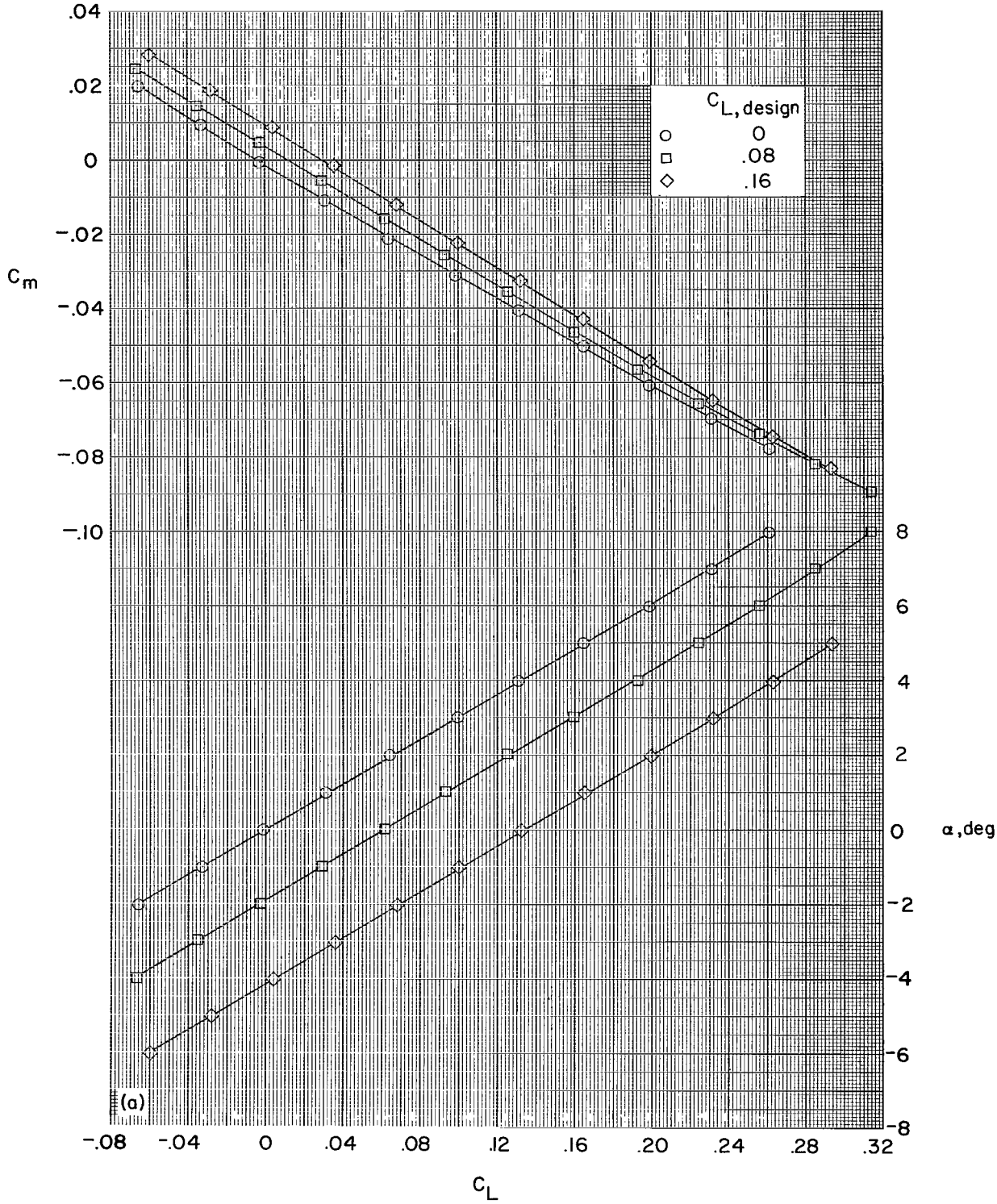

Figure 4.- Measured aerodynamic characteristics in pitch for the K = 1.375 wings.

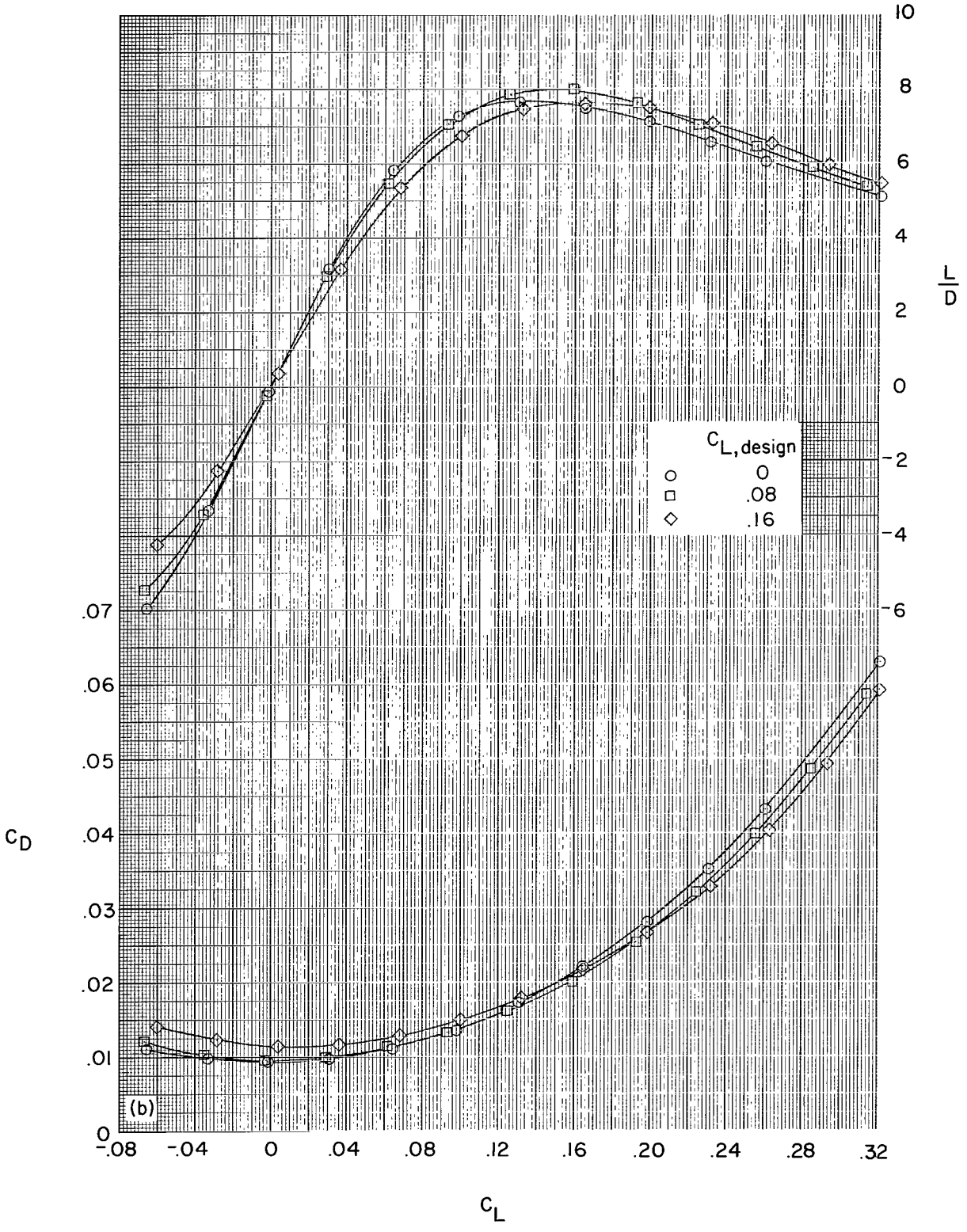

Figure 4.- Concluded.

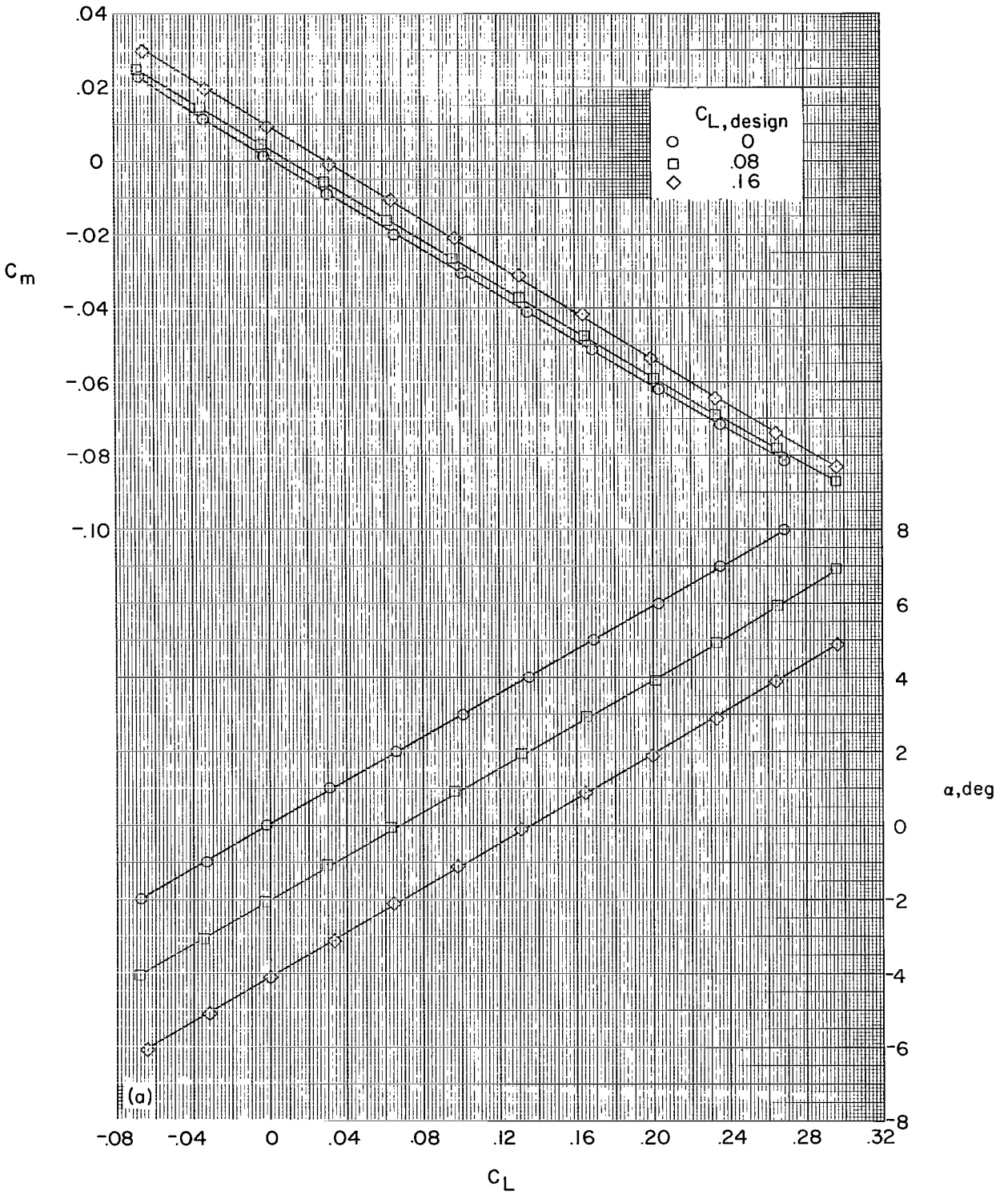

Figure 5.- Measured aerodynamic characteristics in pitch for the K = 1.750 wings.

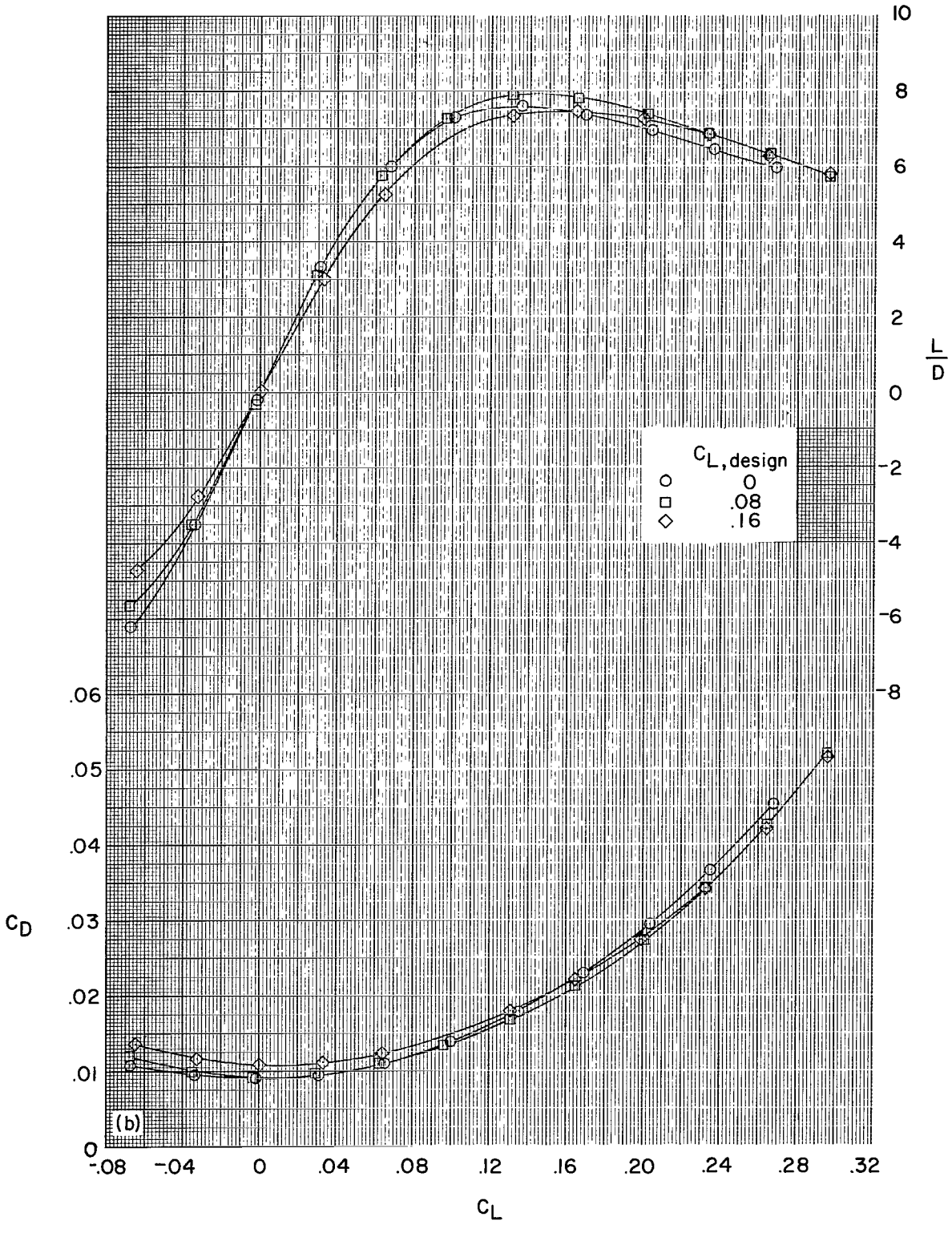

Figure 5.- Concluded.

Comparison With Theory

The variation of drag coefficient with lift coefficient can be estimated by using the method of reference 3 for the zero-lift wave drag, the method of reference 4 for skin-friction drag, and the method of reference 2 for the drag-due-to-lift increment.

Figure 6 shows the estimated drag polars and the wind-tunnel data for both series of wings. Failure of the estimated polars for the two flat wings to match the wind-tunnel data is primarily due to the zero-lift drag estimate being less than the measured value. For the twisted and cambered wings, rather large discrepancies are shown, especially for the wings with the highest design lift coefficient. The minimum drag points on the theoretical curves are seen to occur well above $C_L = 0$; whereas, for the experimental data, the minimum drag point is very close to $C_L = 0$. The theory apparently predicts an amount of asymmetry of the drag polar with respect to $C_L = 0$ which is not present in the experimental data. It is this offset between the experimental and theoretical polars, as well as some discrepancy in the zero-lift drag prediction, which leads to the lack of correlation between theoretical and experimental data. This same type of disparity between theoretical and experimental data can also be noted for the arrow wings of reference 1. Although the steep surface slopes of the arrow wings may lead to flow separation and thus account for part of the lack of correlation, the less severe surface slopes for curved-leading-edge wings probably preclude this line of reasoning. For the arrow wings with a subsonic leading edge, there is a possibility of some beneficial effects from leading-edge thrust and/or a detached vortex flow (see ref. 5), neither of which is considered in the theory. For the curved-leading-edge wings, which have a considerable portion of the leading edge forward of the Mach line, these effects are probably not present.

A comparison between the theoretical and experimental maximum lift-drag ratio for both families of wings is shown in figure 7. It can be seen from the theoretical curves that the highest rate of increase in $(L/D)_{max}$ occurs between the flat wing and the wing designed for a lift coefficient of 0.08, with only a slight increase beyond a design lift coefficient of 0.08. For the real wings, an increase in maximum lift-drag ratio for a design lift coefficient of 0.08 is realized whereas a significant drop occurs in maximum lift-drag ratio for a design lift coefficient of 0.16. However, in no case does the real cambered wing attain its potential.

The variation of $(L/D)_{max}$ with design lift coefficient for the curved-leading-edge wings is essentially the same as for the arrow wings of reference 1; the highest lift-drag ratios were measured for the wings which were designed for a lift coefficient well below that for $(L/D)_{max}$. For the wings designed for a lift coefficient near that for $(L/D)_{max}$, no improvement over the values for the uncambered wings is shown.

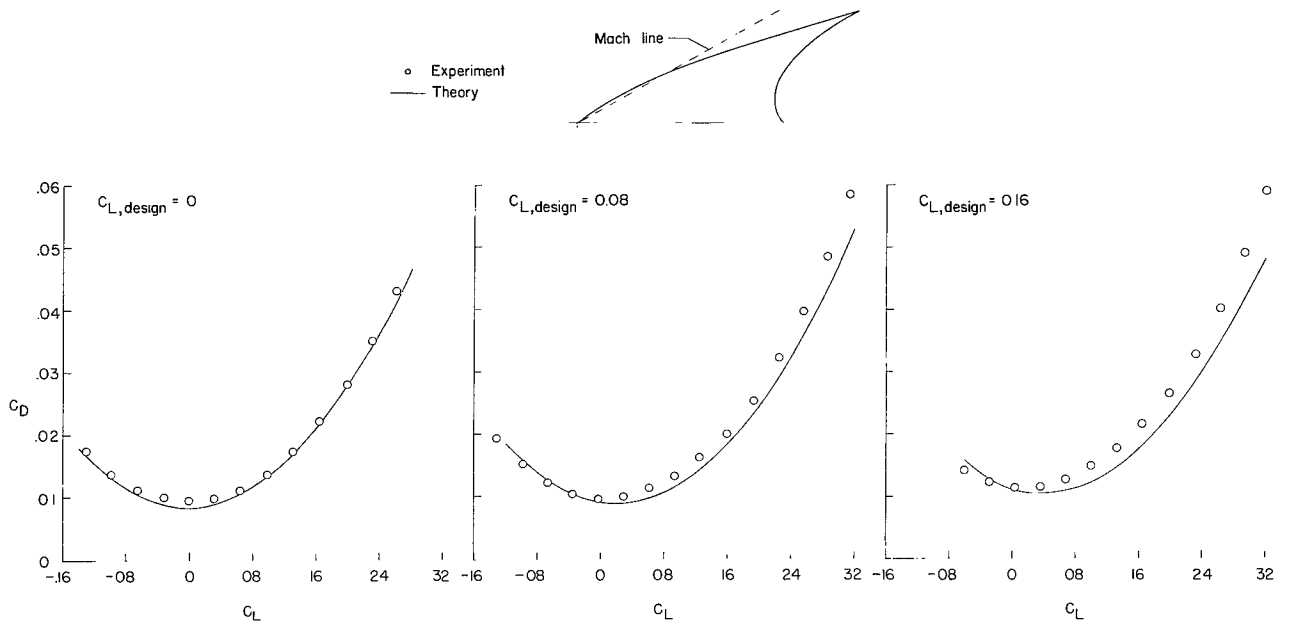

(a) K = 1.375.

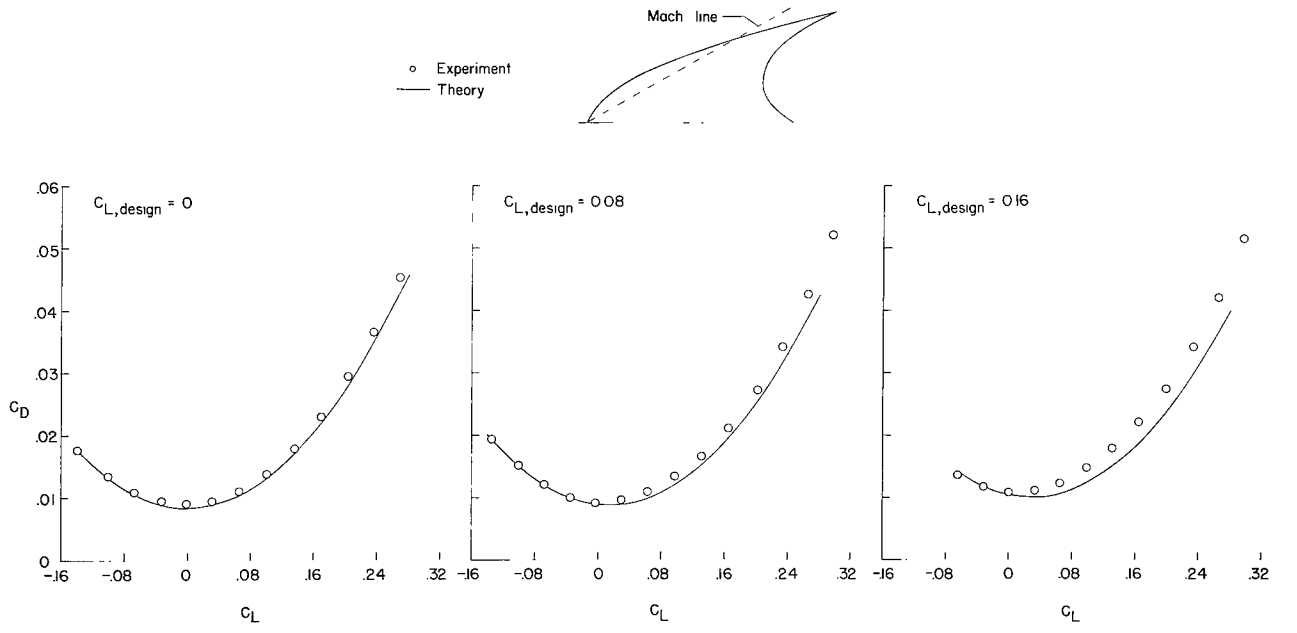

(b) K = 1.750.

Figure 6.- Comparison of theoretical and experimental variation of drag coefficient with lift coefficient.

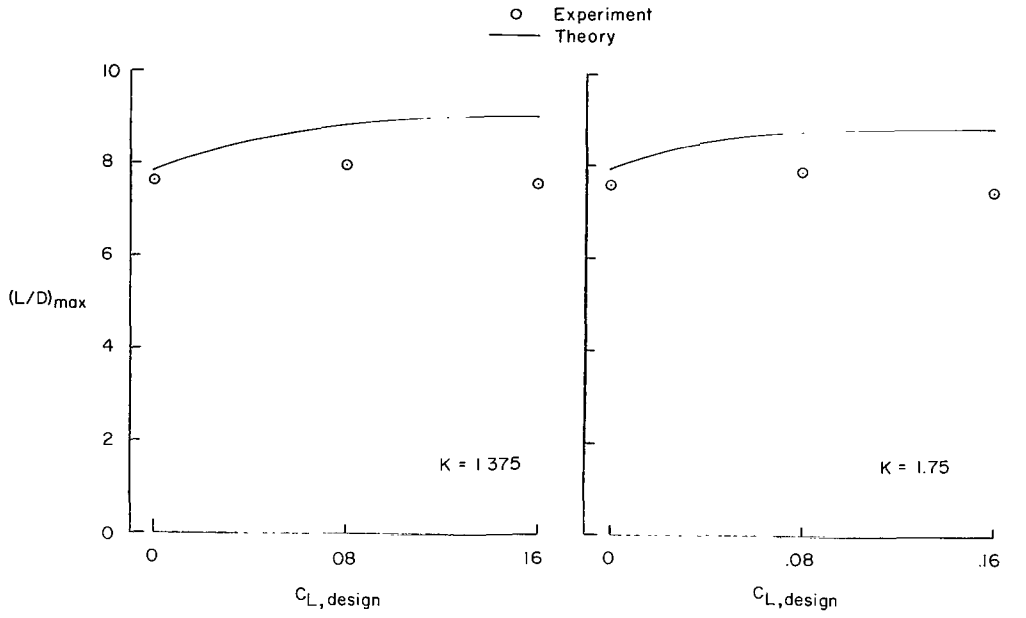

Figure 7.- Maximum lift-drag ratio as a function of design lift coefficient.

Comparison Between Planforms

Some further insight into the characteristics of the curved-leading-edge planforms may be gained by comparing some of the aerodynamic parameters with those for the 70^{o} leading-edge-sweep arrow wings of reference 1. The experimental drag polars for the six curved-leading-edge wings and the three arrow wings are shown in figure 8. The polars are grouped as a function of design lift coefficient. For the flat wings (design lift coefficient equals 0), the arrow wing ($K = 1.000$) has the lowest zero-lift drag; whereas, the $K = 1.375$ wing has the highest value of zero-lift drag. Because the chord distribution and thus the skin friction drag is constant for all the wings, the difference in zero-lift drag for the flat wings is due to differences in the wave drag of the wings and, as such, may change at other Mach numbers. Of particular significance are the drag polars for the wings with design lift coefficients of 0.08 and 0.16. The drag at the higher lift coefficients is seen to be significantly less for the arrow wings than for either of the curved-leading-edge planforms.

The variation of the lift-curve slope with planform exponent K is presented in figure 9. The upward trend of the theoretical lift-curve slope with increasing K is also shown by the experimental results, although the theoretical levels are not attained experimentally.

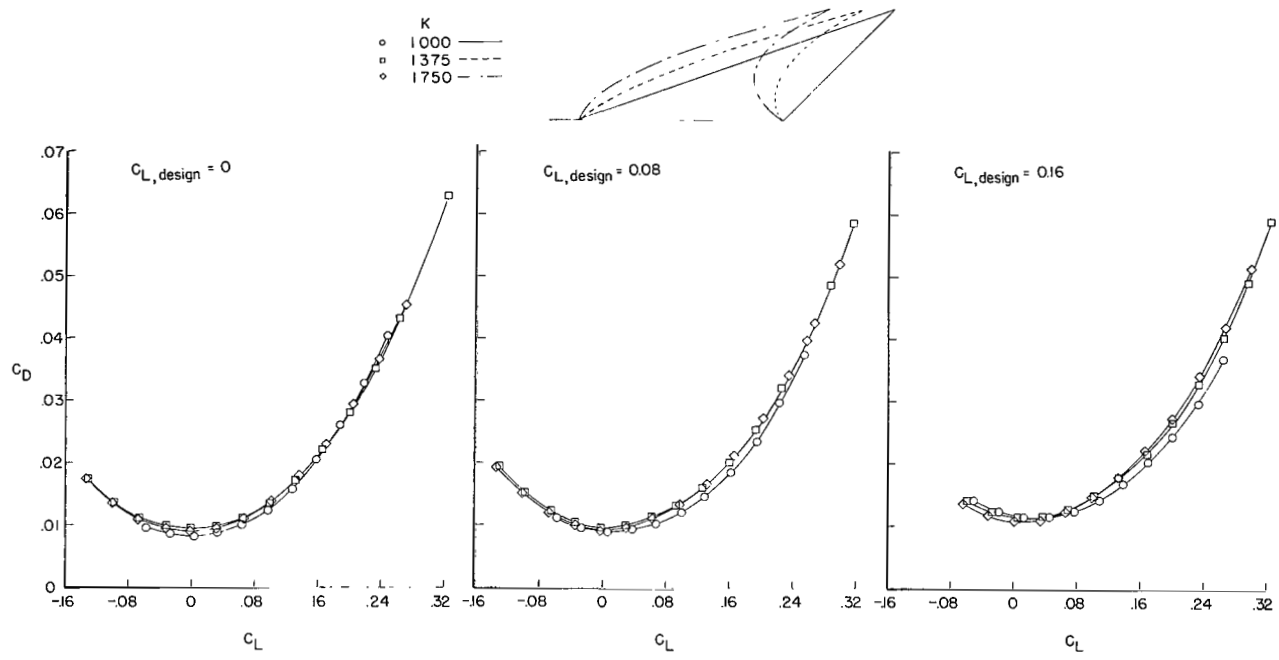

Figure 8.- Comparison of variation of drag coefficient with lift coefficient for all wings.

The static longitudinal stability parameter $\frac{\partial C_m}{\partial C_L}$ as a function of planform exponent K is shown in figure 10. The solid line shows the predicted stability levels whereas the measured data are shown by the symbols. Although the agreement between the theoretical and experimental data is not exact, the trend of increasing stability with increasing K is shown both by theory and experiment. An increase in stability of about 2 percent $\bar{c}$ is obtained as K increases from 1.000 to 1.750.

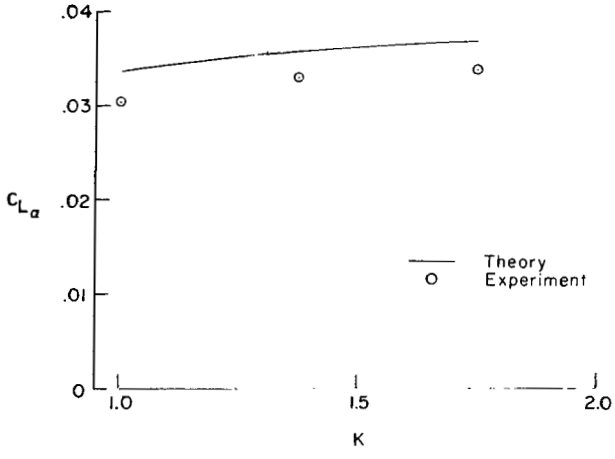

Figure 9.- Variation of lift-curve slope with K.

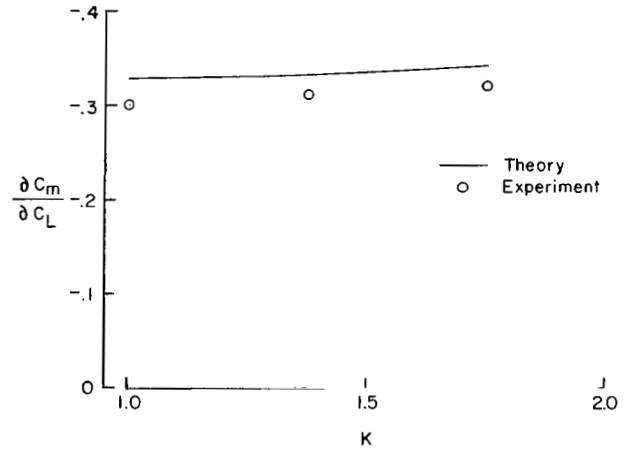

Figure 10.- Variation of static longitudinal stability parameter with K.

The variation of zero-lift pitching-moment coefficient $C_{m,o}$ with planform exponent K is shown in figure 11 for the various design lift coefficients. Also shown are the estimated levels. Some differences between the experimental data and the estimated values can be noted; however, these variations are mostly within the quoted accuracy of the data. The beneficial effects of wing twist and camber in producing desirable levels in $C_{m,o}$ are clearly shown in the figure.

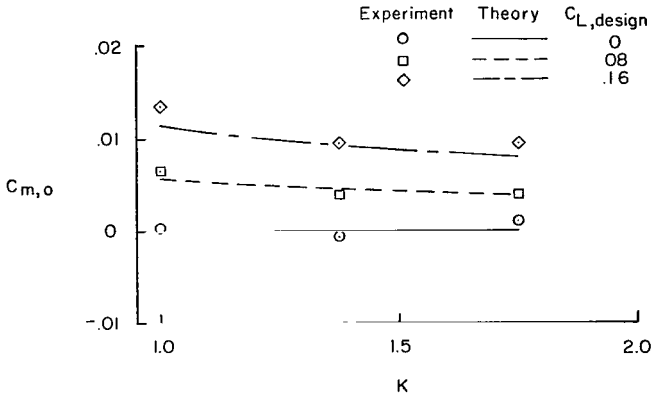

Figure 11.- Variation of zero-lift pitching-moment coefficient with K.

The variation of the drag-due-to-lift factor $\frac{\Delta C_D}{\Delta C_L{}^2}$ with planform exponent K is shown in figure 12 for various design lift coefficients. For comparison, the drag-due-to-lift factor for a wing with no leading-edge suction $\left(\frac{1}{57.3 C_{L_{\alpha,exp}}}\right)$ is shown. The design camber envelope shown represents the value of the drag-due-to-lift factor for a theoretical polar which passes through the design points for each design lift coefficient. Although the polar has no physical meaning, because it includes values for three different camber surfaces, it does provide a lower bound of the drag-due-to-lift factor for camber surfaces designed subject to the restrictions of the design method. (See ref. 2.) The optimum camber curve shows the theoretical drag-due-to-lift factors for another type of envelope polar. This polar is for the whole range of camber-surface shapes over the

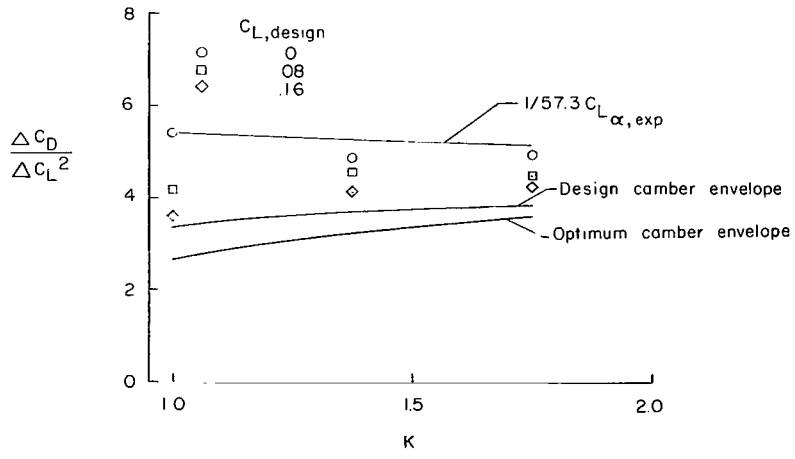

Figure 12.- Variation of drag-due-to-lift factor with K.

lift-coefficient range with no restrictions on pressure coefficients and surface slopes. The drag-due-to-lift factor for this polar represents the maximum potential of the planform which can theoretically be obtained by using twist and camber.

The data points for the various wings were obtained from the linear portion of a plot of C_D as a function of $C_L{}^2$. These values all fall within the two boundaries – that is, $\frac{1}{57.3C_{L_{\alpha,\exp}}}$ as an upper bound and the design camber envelope as a lower bound. It will be noted that the drag-due-to-lift factors for the three wings designed for a lift coefficient of 0.16 closely approach the design camber envelope and these wings would be expected to yield the high values of maximum lift-drag ratio predicted by theory. However, the aforementioned offset between the theoretical and experimental drag polars, as well as the fact that experimental values of $C_{D,o}$ were larger than predicted, resulted in a significant decrement in the performance potential of these $C_{L,\text{design}} = 0.16$ wings.

CONCLUDING REMARKS

An investigation has been conducted in the Langley 4- by 4-foot supersonic pressure tunnel of a series of constant-thickness-ratio wings having curved leading edges and various degrees of twist and camber. The following conclusions are noted:

1. Reduction of design surface slopes by using curved-leading-edge planforms in an attempt to obtain the performance levels predicted by theory did not yield the desired results.

2. The variations of experimental and theoretical maximum lift-drag ratio with design lift coefficient which were noted for an arrow-wing family in an earlier investigation (NASA TM X-332) were essentially duplicated for the two curved-leading-edge families of this investigation; that is, although the theoretical maximum lift-drag ratio increased with increasing design lift coefficient up to 0.16 (the highest design lift coefficient considered), the highest experimental maximum lift-drag ratio occurred for the wings with a design lift coefficient of 0.08.

3. Correlation of the drag data was characterized by an offset between the theoretical and experimental drag polars for the twisted and cambered wings. In addition, a slight difference between the predicted and measured values of zero-lift drag occurred.

4. Comparison of the variation of some of the aerodynamic parameters with planform exponent K (which indicates the amount of curvature in the leading edge) showed an increase in lift-curve slope and a slight increase in stability with increasing K. In addition, the zero-lift pitching moment decreased slightly with increasing K for the twisted and cambered wings.

Langley Research Center,
National Aeronautics and Space Administration,
Langley Station, Hampton, Va., October 18, 1966,
720-01-00-04-23.

REFERENCES

1. Carlson, Harry W.: Aerodynamic Characteristics at Mach Number 2.05 of a Series of Highly Swept Arrow Wings Employing Various Degrees of Twist and Camber. NASA TM X-332, 1960.

2. Carlson, Harry W.; and Middleton, Wilbur D.: A Numerical Method for the Design of Camber Surfaces of Supersonic Wings With Arbitrary Planforms. NASA TN D-2341, 1964.

3. Harris, Roy V., Jr.: An Analysis and Correlation of Aircraft Wave Drag. NASA TM X-947, 1964.

4. Sommer, Simon C.; and Short, Barbara J.: Free-Flight Measurements of Turbulent-Boundary-Layer Skin Friction in the Presence of Severe Aerodynamic Heating at Mach Numbers from 2.8 to 7.0. NACA TN 3391, 1955.

5. Carlson, Harry W.: Pressure Distributions at Mach Number 2.05 on a Series of Highly Swept Arrow Wings Employing Various Degrees of Twist and Camber. NASA TN D-1264, 1962.

"The aeronautical and space activities of the United States shall be conducted so as to contribute . . . to the expansion of human knowledge of phenomena in the atmosphere and space. The Administration shall provide for the widest practicable and appropriate dissemination of information concerning its activities and the results thereof."

—NATIONAL AERONAUTICS AND SPACE ACT OF 1958

NASA SCIENTIFIC AND TECHNICAL PUBLICATIONS

TECHNICAL REPORTS: Scientific and technical information considered important, complete, and a lasting contribution to existing knowledge.

TECHNICAL NOTES: Information less broad in scope but nevertheless of importance as a contribution to existing knowledge.

TECHNICAL MEMORANDUMS: Information receiving limited distribution because of preliminary data, security classification, or other reasons.

CONTRACTOR REPORTS: Technical information generated in connection with a NASA contract or grant and released under NASA auspices.

TECHNICAL TRANSLATIONS: Information published in a foreign language considered to merit NASA distribution in English.

TECHNICAL REPRINTS: Information derived from NASA activities and initially published in the form of journal articles.

SPECIAL PUBLICATIONS: Information derived from or of value to NASA activities but not necessarily reporting the results of individual NASA-programmed scientific efforts. Publications include conference proceedings, monographs, data compilations, handbooks, sourcebooks, and special bibliographies.

Details on the availability of these publications may be obtained from:

SCIENTIFIC AND TECHNICAL INFORMATION DIVISION

NATIONAL AERONAUTICS AND SPACE ADMINISTRATION

Washington, D.C. 20546